Journal of Materials Chemistry A

PAPER

View Article Online
View Journal | View Issue

Cite this: J. Mater. Chem. A, 2014, 2, 1400

Proton incorporation and trapping in ZrO_2 grain boundaries

James A. Dawson* and Isao Tanaka

Received 8th October 2013
Accepted 24th November 2013

DOI: 10.1039/c3ta14029f

www.rsc.org/MaterialsA

The energetics of water incorporation and proton–dopant association in ZrO_2 grain boundaries, namely Σ 5(310)/[001] and Σ 5(210)/[001], are calculated using atomistic simulation techniques and are compared to results obtained for the cubic bulk material. The interatomic potential set was chosen from those available in the literature on the basis of the best fit to experimental data. Both the calculated hydration energy and the redox reaction energies for cubic bulk ZrO_2 are shown to be high, in agreement with the experiment. In contrast, the hydration energies for oxygen ions in and around the grain boundaries are far lower, while the redox energies are also significantly reduced. Strong binding energies between acceptor dopants and protons in bulk ZrO_2 suggest significant proton trapping. While binding (proton trapping) is still prevalent in the grain boundary structures, the binding energies are generally smaller suggesting that should proton conduction occur it is most likely to occur along the grain boundaries rather than the bulk material. Binding is found to be the strongest for smaller ions like Sc and weaker for larger ions like Gd and La. Comparisons between the results for the two grain boundary structures are also made and the consequences for proton migration are assessed.

Introduction

ZrO_2-based materials are renowned for their high oxide ion conductivity which makes them attractive for a wide range of technological applications including solid oxide fuel cells (SOFCs)[1] and oxygen gas sensors.[2] The high strength and fracture toughness of ZrO_2 also make it useful in dental and medical applications.[3,4] The introduction of aliovalent dopants (usually Y^{3+}) to ZrO_2 stabilises the high temperature (>2650 K) cubic polymorph and also introduces charge compensating oxygen vacancies which are responsible for the high ionic conductivity in the system. The considerable amount of work dedicated to the study of oxygen diffusion in these materials is therefore unsurprising. However, in recent years interest in proton conduction in both the bulk and grain boundary structures of fluorite structured materials like ZrO_2 (ref. 5–8) and CeO_2 (ref. 9 and 10) has also increased. Proton incorporation and trapping in zirconate perovskite oxides also receives significant attention.[11–14] $BaZrO_3$ is a prime candidate for SOFCs because of its good chemical and mechanical stability as well as its high proton conductivity.[12]

It is generally considered that oxygen diffusion at grain boundaries in yttria-stabilised zirconia (YSZ) is hindered by space-charge layers or resistive second phases.[15–17] However, there is an ongoing debate as to whether grain boundaries hinder proton diffusion in these materials. Guo[18] observed high proton mobility in ZrO_2 grain boundaries at low temperatures as a result of the transition from the tetragonal phase to the monoclinic phase. It has been reported for both doped-ZrO_2 and CeO_2 that proton conduction occurs under a wet atmosphere at temperatures below 200 °C when the grain size is below 100 nm.[5,19–21] The fact that protonic conductivity increases dramatically with decreasing grain size had led to the conclusion that protons do migrate at the grain boundaries.[5,20] Park *et al.*[22] used X-ray Photoelectron Spectroscopy (XPS) to confirm a higher proton concentration in YSZ thin films prepared by atomic layer deposition than in YSZ single crystals which also suggests that proton diffusion occurs at grain boundaries in YSZ. Conversely, Scherrer *et al.*[6] observed no proton conductivity at grain boundaries in YSZ nanocrystalline, dense thin films. Proton conduction is, however, observed at low temperatures at the inner surface of the porous films. It has also been suggested that such conductivity in YSZ is a result of internal surfaces produced from cracks and pores.[23]

Data in the literature on the hydration enthalpies of YSZ and undoped ZrO_2 are somewhat limited, and generally considered to be 'close to zero' in YSZ and therefore the proton concentration is small.[24] There are, however, a number of computational and experimental studies on the surface hydration of monoclinic, tetragonal and cubic ZrO_2.[25–28] Two such studies use density functional theory (DFT) and thermodynamic modelling to calculate water absorption energies between −1 and −2 eV for both monoclinic[25] and tetragonal ZrO_2.[26] While there exists a wealth of information on proton trapping in Zr- and Ce-based perovskite oxides[11,12,29,30] in the literature, data for doped ZrO_2 are far more sporadic.

Department of Materials Science and Engineering, Kyoto University, Sakyo, Kyoto, 606-8501, Japan. E-mail: dawson.jamesalexander.2w@kyoto-u.ac.jp

Lattice statics simulations of grain boundaries in ionic solids were first studied in the 1980s with pioneering studies on NiO by Duffy and Tasker.[31,32] While no lattice statics study of protons in undoped ZrO_2 or YSZ grain boundaries exists, there is a considerable amount of simulation work dedicated to oxygen diffusion and dopant segregation in these grain boundaries.[33–37] Molecular dynamics studies by Fisher *et al.*[33] and González-Romero *et al.*[34] showed that for a range of grain boundaries in ZrO_2 and YSZ (including Σ 5) oxygen diffusion is slower and that generally these interfaces act as a source of resistance. Hybrid Monte Carlo-molecular dynamics have been used to confirm high concentrations of oxygen vacancies and significant amounts of dopant segregation at the Σ 5(310)/[001] tilt grain boundary in YSZ and Gd-doped CeO_2.[36] The methods used in this study have also been used to investigate the defect chemistry, proton sites and dopant–proton association in a number of potential proton conducting bulk materials.[12,38–41]

This study uses well established atomistic simulation techniques to answer fundamental questions on the nature of protons in the bulk and grain boundary structures of this technologically essential material. To the best of our knowledge, this is the first study to apply these techniques to the investigation of protons in grain boundaries in any material. Hydration enthalpies, redox properties and proton trapping effects are calculated and discussed. Comprehensive comparisons are made between the bulk material and the grain boundaries as well as between the two types of grain boundaries themselves. Comparison with experiments is made wherever possible. This investigation will encourage similar work on doped systems (*e.g.* YSZ) and more complex systems such as proton conducting perovskites as well as the calculation of proton migration energies and pathways in these materials.

Simulation methods

The inter-ionic interactions in this work are simulated using the Born model for ionic solids. In this model interactions between ions are accounted for by short-range forces in the form of spherical interatomic potentials and long-range forces which are treated using Coulombic terms. The methods discussed in this section are very well established and comprehensive reviews are available elsewhere.[42] Numerous potential models are available for ZrO_2, each with its own individual strengths and weaknesses. For this study we have chosen the potential set developed by Woodley *et al.*[43] as this model has the best agreement with the experimental lattice parameter and lattice energy of cubic ZrO_2, as shown in Table 1. While all the potential models tested reasonably reproduce the ZrO_2 structure, it is clear that the Woodley *et al.*[43] potential set is the most accurate. The experimental lattice energy was calculated using energy of the formation cycle. The values for this cycle can be found in the literature.[44–46] The interatomic potentials used to model ZrO_2 in this work take the Buckingham form:

$$V_{ij}(r) = \sum_{i \neq j}^{n} A\exp\left(-r_{ij}/\rho\right) - \frac{C}{r_{ij}^6} \quad (1)$$

Table 1 Experimental and calculated lattice constants and energies for cubic ZrO_2

	Lattice constant (Å)	Lattice energy (eV)
Experiment[43–47]	5.09	−114.53
Woodley *et al.*[43]	5.07	−113.80
Lewis and Catlow[48]	5.14	−110.88
Minervini *et al.*[49]	5.12	−111.11

where the symbols have their usual meanings. Both the Zr and O ions are assumed to be fully ionic and therefore have formal charges. A cutoff of 10 Å was applied to all of the potentials.

All point defects and dopant ions are simulated at the infinitely diluted limit using the Mott and Littleton method.[50] In this approach the area surrounding the defect is divided into an inner and outer region. In the inner region atomic interactions are calculated explicitly, whereas in the outer region (where the interactions are weaker) they are approximated using a dielectric continuum method:

$$E = E_1(x) + E_{12}(x,\eta) + E_2(\eta), \quad (2)$$

where E_1 and E_2 are the energies of the inner and outer regions, respectively and E_{12} is the energy of the interactions between them. Atomic displacements are denoted by x and η for the inner and outer regions, respectively. Beyond the inner region, a uniform material that relaxes harmonically based on its dielectric constant and structure is assumed. This is not the case for grain boundary structures. However, given that the structure is cubic it is unlikely that this effect is significant. This is also confirmed by rigorous testing of the energy convergence with the Mott–Littleton region sizes completed for this work. All the calculations in this work were completed using the General Utility Lattice Program (GULP).[51]

For the interactions of the protons we use an attractive Morse potential developed using *ab initio* cluster calculations[52] to describe the O–H interaction as well as a Buckingham potential to describe the interactions between the OH group and the surrounding lattice.[53] The Morse potential takes the form:

$$V(r) = D\{1 - \exp[-\beta(-r/r_0)]\}^2 \quad (3)$$

where D, β and r_0 are the parameters obtained from *ab initio* quantum mechanical cluster calculations with a point charge representation of the surrounding lattice.[52] In order to give the OH group the correct overall charge of −1, the dipole is distributed across both ions with an oxygen charge of −1.4263 and a hydrogen charge of +0.4263. This approach has been successfully applied to a wide range of materials.[12,38–41,54]

Results and discussion

Grain boundary structures and energies

Two symmetric tilt grain boundaries, Σ 5(310)/[001] and Σ 5(210)/[001], were examined in this study. Fig. 1 shows the starting unoptimised structures of the two ZrO_2 grain

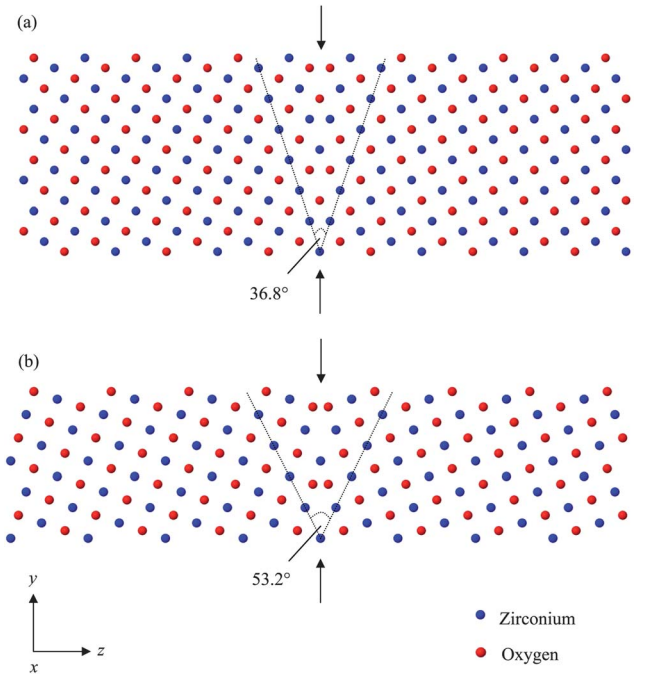

Fig. 1 Initial structures for the (a) Σ 5(310)/[001] and (b) Σ 5(210)/[001] grain boundaries. The arrows indicate the position of the grain boundary in the supercell.

boundaries. These grain boundaries were formed using the CSL theory where two individual grains are tilted by a given angle (36.8° for Σ 5(310)/[001] and 53.2° for Σ 5(210)/[001]) until their surface planes ((310) or (210)) coincide. Both of these grain boundaries have been studied experimentally using transmission electron microscopy (TEM)[55] and high resolution electron microscopy (HREM)[56] which allows for direct comparison. Both of the grain boundary supercells are longest in the z direction in order to minimise the interactions between the equivalent grain boundaries at the centre and edges of the supercells.

One issue with the starting configurations of these symmetrical grain boundaries is that ions with the same charge are in a closer proximity. This leads to increased Coulombic repulsion and high grain boundary energies. One solution to this issue proposed by Yoshiya *et al.*[37] is to introduce vacancies across the grain boundary and halve the atom density. In this work, we address the issue by exploring the γ surface of the grain boundaries. Using rigid body translations, one grain can be displaced with respect to the other in various three-dimensional translation states. This method is crucial in finding the global minimum and works by calculating the grain boundary energy at each translation. The grain boundary is calculated by:

$$\sigma_{GB} = \frac{E_{GB} - E_{bulk}}{2A} \quad (4)$$

where E_{GB} and E_{bulk} are the energies of the grain boundary and the bulk supercell respectively, and A is the area of the interface. The area of the interface is doubled to account for the presence of the two equivalent grain boundaries in the supercell. The energy was calculated as a function of translation states with increments of about 0.01 nm. A similar approach was used for atomistic simulations of ZnO grain boundaries.[57,58] Table 2 shows the lowest calculated grain boundary energy for each grain boundary and the respective translations and cell physical dimensions. Fig. 2 illustrates the fully optimised, lowest energy configurations of the two grain boundaries used in this study.

The most obvious difference between the optimised structures in Fig. 2 and the initial structures in Fig. 1 is the open channels at the grain boundaries in the optimised cells. Given the significant Coulombic repulsion present between the ions at the grain boundaries in the initial structures, it is not surprising that such open channels are present as they reduce the atom density in the grain boundaries and therefore reduce the strain caused by the repulsion. This open channel structure is not observed experimentally for the Σ 5(310)/[001] grain boundary in YSZ.[55,59] Instead the grain boundary core contains a single zirconium column as opposed to the two zirconium columns present in the CSL model structure. However, lattice statics calculations by Shibata *et al.*[60] do show significant grain boundary expansion in YSZ [110] grain boundaries. It has been reported that it is the presence and segregation of Y in these grain boundaries that removes such open channels in YSZ by the formation of one fully occupied column.[35,37]

In the bulk cubic ZrO_2 structure Zr has eightfold coordination and O has fourfold coordination, this is reduced at the grain boundary core. For both boundary cores, the coordination of Zr is reduced to sixfold and O is threefold-coordinated. At the layers directly surrounding the grain boundaries the coordination of Zr remains sixfold whereas for O a mixture of threefold and fourfold is observed before the coordination environment of both ions returns to the usual values in the bulk-like structure beyond the grain boundaries. The calculated grain boundary energies are in good agreement with previous computational work.[33,37] Yoshiya *et al.*[37] calculated energies of 2.52 J m^{-2} for Σ 5(310)/[001] and 2.69 J m^{-2} for Σ 5(210)/[001]. These energies are lower than our calculated values, although this is to be expected as the approach of removing ions from the grain boundaries to reduce Coulombic repulsion was not taken here. Fisher and Matsubara[33] used molecular dynamics to calculate a value between 2.7 and 2.9 J m^{-2} for the Σ 5(310)/[001] boundary at temperatures between 1273 and 2673 K. Our grain boundary energy values were obtained from supercells with 336–360 atoms. Convergence with grain boundary separation was tested and achieved using a selection of supercells with fewer atoms and smaller z cell dimensions.

Redox reactions

The redox properties of a proton conductor are important as their applications often require them to remain stable and work over a wide range of oxidising and reducing conditions. By calculating and comparing these properties both for the bulk material and its grain boundaries, we can make an assessment on the effect the grain boundaries have on the application of this material as a potential proton conductor.

Table 2 Lowest grain boundary energies for the two structures and the respective translations, cell dimensions and grain boundary separations

Grain boundary	Energy (J m^{-2})	Translation displacement			Cell dimensions (x, y, z) (Å)	Grain boundary separation (Å)
		t_x (frac.)	t_y (frac.)	t_z (Å)		
Σ 5(310)/[001]	3.23	0.22	0.14	1.00	5.07, 16.03, 50.30	25.15
Σ 5(210)/[001]	3.27	0.29	0.12	0.90	5.07, 11.34, 65.49	32.75

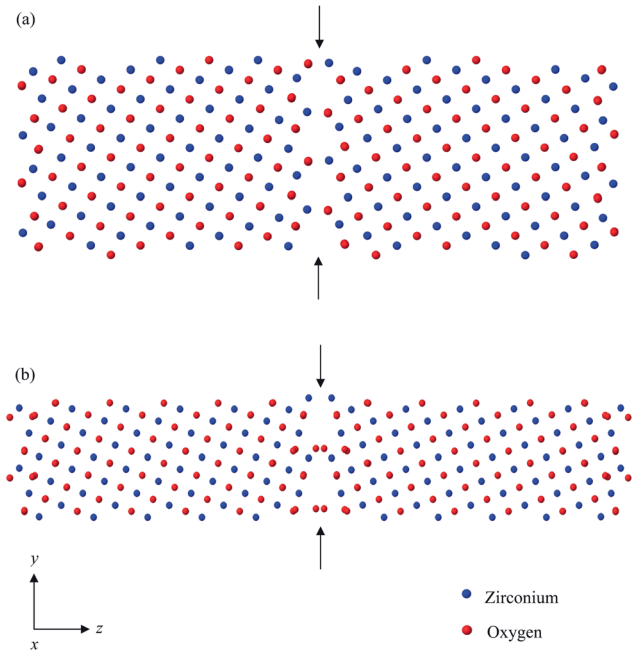

Fig. 2 Optimised structures for the (a) Σ 5(310)/[001] and (b) Σ 5(210)/[001] grain boundaries. The arrows indicate the position of the grain boundary in the supercell.

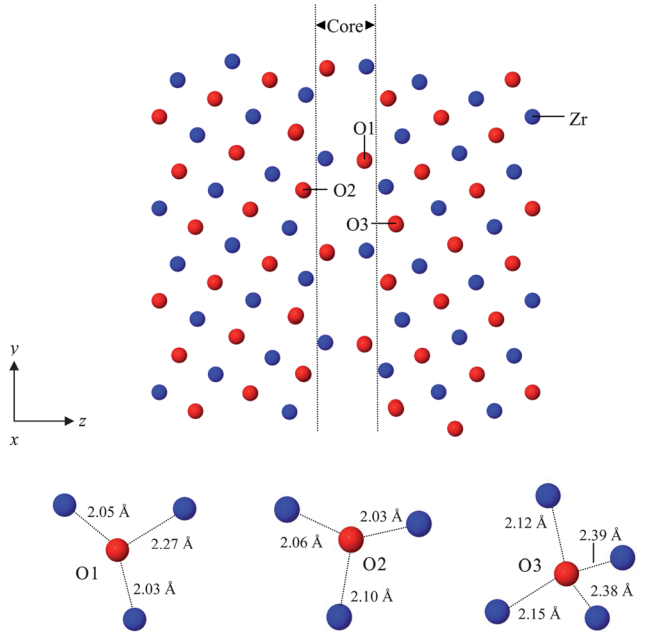

Fig. 3 Schematic of the three oxygen environments investigated in the Σ 5(310)/[001] grain boundary. O1 is in the grain boundary core, while O2 and O3 are in the adjacent grain boundary layers.

The reaction for reduction involves the formation of oxygen vacancies which are compensated for by electronic defects (namely the reduction of M^{4+} to M^{3+}):

$$O_O^x \rightarrow V_O^{\cdot\cdot} + \frac{1}{2}O_{2(g)} + 2e' \quad (5)$$

For oxidation we assume oxygen vacancies are already present in the system as a result of acceptor doping:

$$V_O^{\cdot\cdot} + \frac{1}{2}O_{2(g)} \rightarrow O_O^x + 2h^{\cdot} \quad (6)$$

where $h^{\cdot}$ is an electron hole. Both the electronic defects and electron holes are treated as small polarons localised at ion sites meaning holes ($h^{\cdot}$) are modelled as O^- ions substituted at O^{2-} sites and electronic defects (e') are modelled as M^{3+} ions substituted at M^{4+} sites. These substitutions are modelled using the same interatomic potentials and the ionic charge is changed by one. These energies are calculated for bulk ZrO_2 and three different oxygen environments (Fig. 3 and 4) in each grain boundary and are then combined with the appropriate ionisation energy or electron affinity term and are presented in Table 3. These values are summed with the relevant electronic terms to obtain the energies of the redox reactions and are given in Table 4. Detailed analysis of these values must be treated with some care because of the uncertainties in the free-ion terms used. The values do, however, provide a good insight into the general trends and are useful for comparison between different materials and structures.

Fig. 3 and 4 illustrate the O ions used for the calculation of the redox reactions in the grain boundaries. The first ion (O1) was chosen from the grain boundary core, the second ion (O2) was chosen from the first adjacent grain boundary layer and the final ion (O3) was chosen from the second adjacent layer. The values show that reduction is energetically favoured over oxidation in the system, but generally the energy for both oxidation and reduction is high. It is also clear that oxidation and reduction are significantly favoured at the grain boundary core and the first adjacent layer. Unfortunately, experimental data on the redox energies of ZrO_2 and YSZ are limited at best. The energies for reduction at the grain boundaries are, however, comparable with experimental values of CeO_2 (ref. 61) and Sm-doped CeO_2.[62] The preference of reduction *via* the production of oxygen vacancies and electrons over oxidation suggests the dominance of n-type electronic conductivity over p-type electronic conductivity in the undoped material, as supported by experiments[63–65] and observed for the proton conductor

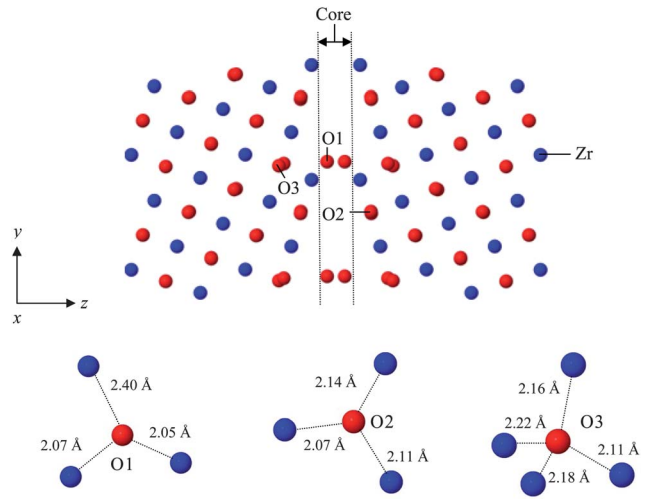

Fig. 4 Schematic of the three oxygen environments investigated in the Σ 5(210)/[001] grain boundary. O1 is in the grain boundary core, while O2 and O3 are in the adjacent grain boundary layers.

Table 3 Energies of electronic defects in the bulk and grain boundary structures of ZrO_2

	Energy (eV)						
	Bulk	Σ 5(310)/[001]			Σ 5(210)/[001]		
Defect	O	O1	O2	O3	O1	O2	O3
O^- ($h^\bullet$)	8.78	7.72	7.08	8.48	8.20	7.12	9.50
Zr^{3+} (e')[a]	4.04	3.54	4.34	3.54	3.62	3.62	3.62

[a] Calculated for the Zr ion closest to the O ion of interest.

Table 4 Energies of redox reactions in the bulk and grain boundary structures of ZrO_2

	Energy (eV)						
	Bulk	Σ 5(310)/[001]			Σ 5(210)/[001]		
Defect	O	O1	O2	O3	O1	O2	O3
Oxidation	6.32	4.98	5.38	5.56	5.12	4.88	6.54
Reduction[a]	5.47	4.61	4.26	5.53	5.03	4.37	5.02

[a] The reduction energies are calculated using a bound $E^{Zr^{3+}}_{sub,Zr} - V_O^{\cdot\cdot} - E^{Zr^{3+}}_{sub,Zr}$ defect cluster.

$BaCeO_3$.[66] At the grain boundary core, oxidation and reduction are both favoured in the Σ 5(310)/[001] grain boundary more than in the Σ 5(210)/[001] grain boundary. These results suggest that a larger concentration of electronic defects exists at the grain boundaries compared to the bulk material.

Proton incorporation

Proton incorporation can be achieved in these materials through treatment with water vapour. Oxygen vacancies usually formed to compensate the negative charge formed from acceptor doping are replaced by the protonic defects[6,12,63] as illustrated by:

$$H_2O + O_O^x + V_O^{\cdot\cdot} \rightarrow 2OH_O^{\cdot} \quad (7)$$

where the protonic defect is described as a hydroxyl ion.

Protonic conduction in ZrO_2 is attributed to the Grotthuss mechanism[6,21,67] where protons 'hop' between neighbouring oxygen ions. Quantum mechanical computational studies on proton conduction in perovskites also suggest that rotational movement of the hydroxyl group and potential quantum tunnelling are also important in the process.[12,68,69] Therefore, calculations to determine the correct O–H configuration are essential.

Fig. 5 and 6 show the calculated lowest energy O–H configurations for the bulk structure and for the O ions of interest in

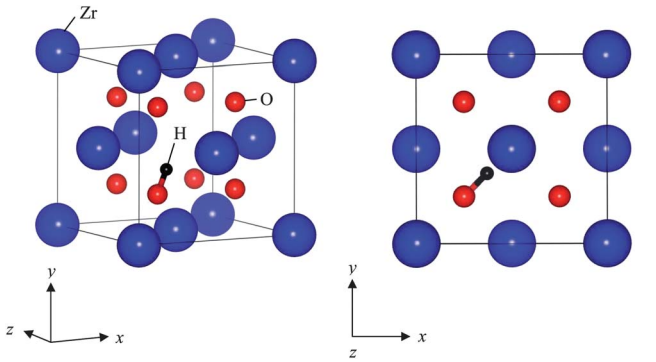

Fig. 5 Schematic of the lowest energy O–H configuration in cubic bulk ZrO_2.

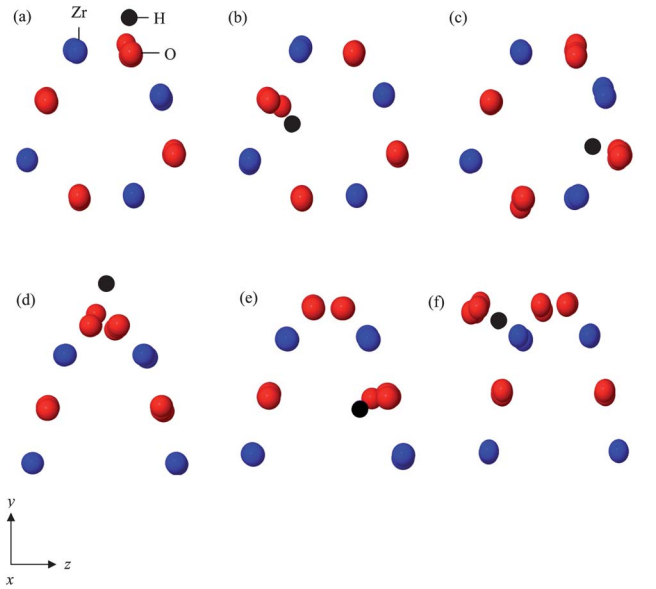

Fig. 6 Schematic of the lowest energy O–H configurations in the Σ 5(310)/[001] and Σ 5(210)/[001] grain boundaries (a) Σ 5(310)/[001] O1, (b) Σ 5(310)/[001] O2, (c) Σ 5(310)/[001] O3, (d) Σ 5(210)/[001] O1, (e) Σ 5(210)/[001] O2 and (f) Σ 5(210)/[001] O3.

both the grain boundaries. For the bulk structure, the equilibrium proton position lies directly between the bonded O ion and the central point of the cell. In this position the proton lies at the maximum distance away from any of the surrounding Zr ions, thus minimising Coulombic repulsion. An O–H distance of 0.99 Å is observed, in agreement with typical values found in Zr-based perovskite proton conductors.[12] Fig. 6 clearly shows the local distortion in the lattice caused by the introduction of the proton. Where possible the H atom prefers to reside inside the open channels of the grain boundary. Another interesting feature of these proton doped grain boundaries is the ability for the H atom to displace the bonded O ion from its lattice site. Again the position of the H atoms is where Coulombic repulsion from the Zr ions is at a minimum. The only exception to this is perhaps the O3 ion in the Σ 5(210)/[001] grain boundary, where it is more difficult for the H atom to position itself in the grain boundary core.

The hydration energy (E_{H_2O}) is based on eqn (7) and is calculated using:

$$E_{H_2O} = 2E_{OH} - E(V_O^{\cdot\cdot}) + E_{PT} \quad (8)$$

where E_{OH} is the energy associated with the substitution of an O^{2-} ion with an OH^- group, $E(V_O^{\cdot\cdot})$ is the oxygen vacancy energy and E_{PT} is the energy of the gas phase reaction $O^{2-} + H_2O = 2OH^-$. This final term can be estimated from the difference between the proton affinity of O^{2-} and OH^- and is taken to be −11.77 eV in this work.[70] A more detailed explanation of this approach is available elsewhere.[71,72]

The calculated hydration energies and other relevant terms are given in Table 5. An interesting feature of this data is the large spread of values for the oxygen vacancy energies. For the O ions in the first grain boundary layer adjacent to the core (O2) the values are significantly lower when compared to the bulk and other grain boundary O ions, this is especially in the case of O2 in the Σ 5(310)/[001] grain boundary. This is most likely a result of the strain caused by the unfavourable O threefold coordination and the fact that the Zr–O interatomic distances are significantly smaller (Fig. 3 and 4) than the Zr–O distance in the bulk material. The oxygen vacancies energies are higher in the Σ 5(210)/[001] grain boundary than in the Σ 5(310)/[001] grain boundary. All of the E_{OH} values calculated for the grain boundaries O ions (with the exception of O3 in Σ 5(210)/[001]) are significantly lower than the bulk values. This is important as it implies that preferential substitution of the hydroxyl group occurs at the grain boundaries. Similar to the oxygen vacancy energies, the lowest E_{OH} values are observed for the first grain boundary layer.

Table 5 Hydration energies and additional values used in eqn (8) for the bulk and grain boundary structures of ZrO_2

	Energy (eV)						
	Bulk	Σ 5(310)/[001]			Σ 5(210)/[001]		
	O	O1	O2	O3	O1	O2	O3
$E(V_O^{\cdot\cdot})$	14.77	15.34	13.25	15.70	16.02	14.34	15.79
E_{OH}[a]	16.51	14.15	13.74	15.13	15.06	13.78	16.92
E_{H_2O}	6.48	1.19	2.46	2.79	2.33	1.45	6.28

[a] Includes D of the Morse potential (7.05 eV).

In agreement with the hydration energy for YSZ,[24] the hydration energies for ZrO_2 are positive and in the case of the bulk material very high suggesting a low concentration of protons in the material. This is especially true considering the recently calculated hydration enthalpy for CeO_2 of 0.68 eV.[73] However, the difference between the calculated values for the bulk and the grain boundaries is significant. With the exception of O3 in the Σ 5(210)/[001] grain boundary, the hydration energies in both grain boundaries are between 3.69 and 5.29 eV lower than in the bulk. This clearly suggests that the proton concentrations in and around the grain boundaries of cubic ZrO_2 is much higher than in the bulk. It is noteworthy to add that the introduction of aliovalent dopants such as Y will most likely further decrease the hydration energies (and hence increase the proton concentration) as a result of the binding between the dopants and the protons as discussed in the next section. The high hydration energy calculated for O3 in the Σ 5(210)/[001] grain boundary is due to its position respective to the grain boundary core and the fact that this makes it more difficult for the proton to reside in the grain boundary core. As discussed previously, no experimental or computational value for the hydration energy in bulk ZrO_2 could be found making direct comparison difficult. However, regardless of this, these results illustrate the importance of considering grain boundaries when investigating protons in these materials and the dramatic effect they can have on proton incorporation.

Proton–dopant association (proton trapping)

In order for protons to achieve long-range transport, they must overcome any potential proton trapping effects resulting from the association between the protons and aliovalent dopants. While this is fundamentally important to the application of any proton conductor, it is often not fully understood. Numerous experimental and computational studies have been dedicated to the investigation of proton trapping effects in proton conducting materials.[11,12,39] By calculating the binding energies between neighbouring OH groups and aliovalent dopants and by assessing the local relaxations around the defect pair, we provide a detailed assessment of proton trapping effects in bulk ZrO_2 and its grain boundaries. For all structures the closest Zr ion site to the proton was chosen as the dopant substitution site. A wide range of dopants common to this material were tested in order to assess the consequences of substituting with ions of varying ionic radii. Three examples of the relaxed local structures of these defect pairs are presented in Fig. 7.

The binding energy (E_{bind}) between defect clusters is defined as the difference between the total energy of the isolated defects and when the relevant defects are simulated together in a cluster.[74–76] A negative binding energy implies binding behaviour. This energy will have to be overcome along with the usual activation energy by the protons if long-range transport is to occur. Fig. 8 shows the calculated binding energies for each

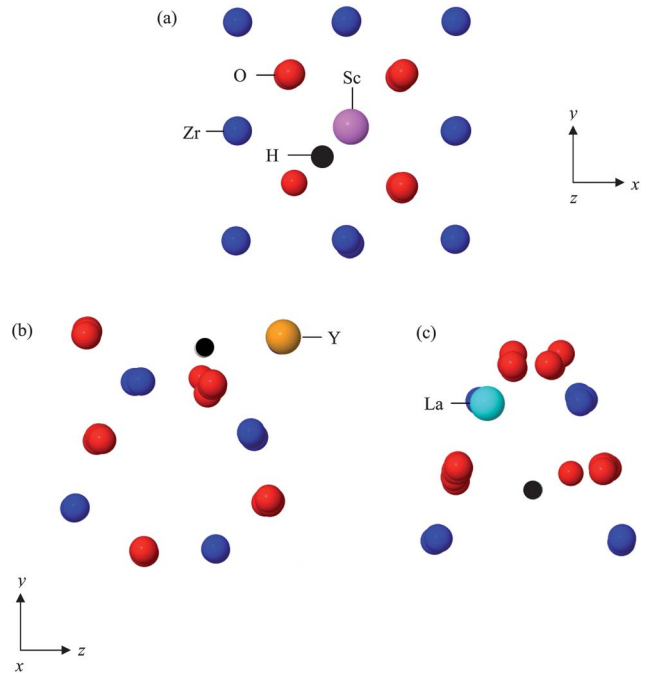

Fig. 7 Relaxed local structures of proton–dopant pairs (a) Sc-doped bulk ZrO_2, (b) Y-doped Σ 5(310)/[001] (O1) and (c) La-doped Σ 5(210)/[001] (O2).

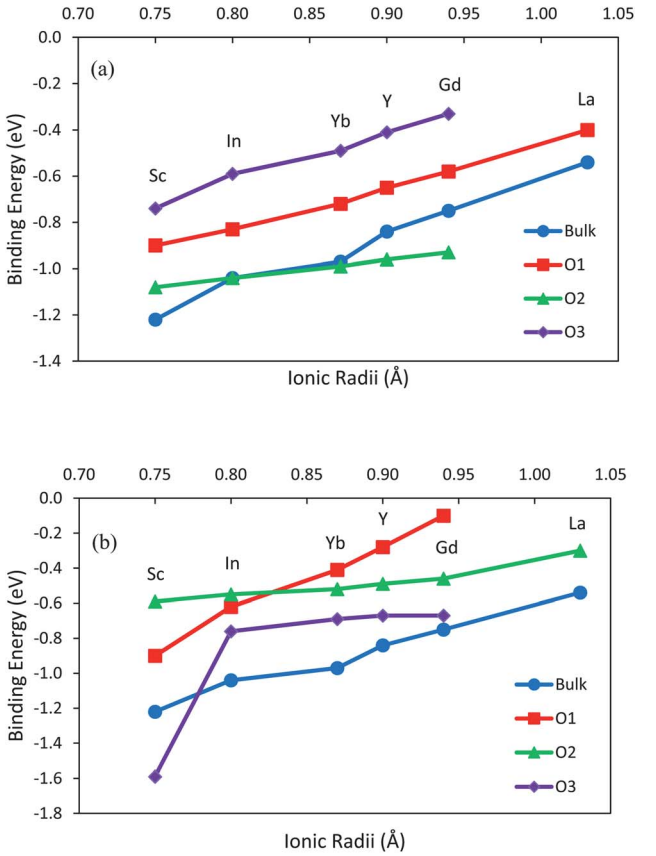

Fig. 8 Comparison of dopant–proton binding energies for a range of dopant ion sizes in bulk ZrO_2 with (a) the Σ 5(310)/[001] grain boundary and (b) the Σ 5(210)/[001] grain boundary. Some binding energies for La doping have been omitted as they are positive in energy and therefore physically unlikely. These values are discussed in the main text.

dopant ion in the bulk and grain boundary structures. The effect of the dopant ions on the local structure is measured by analysing the interatomic distances between the dopant and the proton and the results are given in Table 6.

With the exception of some values for La-doping in the grain boundaries, all the binding energies are negative and therefore their formation is favourable. The magnitude of the binding energy is proportional to the dopant size with the smallest ions (*e.g.* Sc and In) having the strongest association with the proton and the largest ions (*e.g.* Gd and La) having the weakest association. Sc-doped ZrO_2 has received interest because of its superior ionic conductivity compared to YSZ.[77] However, our results show that the highest binding energies were observed for Sc in all structures, suggesting that when doped, the small ionic radius of Sc is responsible for forming a strong association with neighbouring positive defects. The most important dopant used in ZrO_2, Y, has reasonably weak binding in agreement with its ionic radii relative to the other dopants. For La the binding energies are the largest and in some cases strongly positive (Σ 5(310)/[001] O2 – 0.78 eV, Σ 5(310)/[001] O3 – 1.09 eV, Σ 5(210)/[001] O1 – 3.04 eV and Σ 5(210)/[001] O3 – 0.63 eV). Given the significant ion size mismatch between Zr and La, it is not surprising that La has such a strong effect on the surrounding lattice and this is especially true for the grain boundaries. This is also supported by the dopant–proton interatomic distances (Table 6).

Comparison of the binding energies within the grain boundaries and the bulk shows that generally the binding is stronger in the bulk material. This is important as it suggests that should long-range proton transport occur in ZrO_2 it will occur at the grain boundaries, in agreement with experimental results for YSZ.[5,20,22] One obvious reason as to why the binding is weaker in the grain boundary is that usually the dopant–proton distances are larger in the grain boundaries than in the bulk (Table 6), thus limiting the Coulombic attraction. Unfortunately the experimental work on proton trapping in both pure ZrO_2 and YSZ is extremely limited with most effort focused on

Table 6 Dopant–proton (M–H) interatomic distances of the defect pair for the bulk and grain boundary structures of ZrO_2

		M–H (Å)						
		Bulk	Σ 5(310)/[001]			Σ 5(210)/[001]		
Ion	Ionic radius (Å) (ref. 68)	O	O1	O2	O3	O1	O2	O3
Zr	0.72	2.25	2.78	2.80	2.50	2.63	2.60	2.23
Sc	0.75	2.15	2.71	2.46	2.27	2.59	2.91	2.17
In	0.80	2.18	2.76	2.88	2.35	2.58	2.89	2.06
Yb	0.87	2.20	2.88	2.91	2.39	2.59	2.89	2.05
Y	0.90	2.21	2.92	2.94	2.41	2.59	2.89	2.05
Gd	0.94	2.25	2.98	2.97	2.44	2.61	2.87	2.05
La	1.03	2.32	3.11	4.10	2.05	2.87	2.72	2.42

perovskite materials.[12,78] It is hoped that the results presented here will encourage more experimental and computational research into this topic. The majority of our calculated binding energies for the grain boundaries are similar to the values calculated for the perovskite proton conductor, $BaZrO_3$ (~0.2 eV–0.8 eV).[12] However, it is important to note that our values for bulk ZrO_2 are significantly larger than the values calculated for bulk $BaZrO_3$.

With regards to the bulk structure, dopant ions up to the size of Y (0.90 Å) cause a decrease in the M–H distance in agreement with the strong binding energies. Beyond the size of Y (*e.g.* Gd and La), the binding energy is smaller and the size mismatch between Zr and the dopant ions perturbs the surrounding lattice sufficiently enough to hinder the proton from moving closer to the dopant ion. While this trend also exists for O1 in the Σ 5(310)/[001] grain boundary, it is more complex for the other O ions in the grain boundaries. For O ions in the Σ 5(210)/[001] grain boundary there is very little variation in the M–H distances with the exception of La which causes strong perturbations to the lattice because of its large ionic radius. These results confirm that the local structure of any given grain boundary can have a dramatic effect on the nature of the dopant–proton association. By detailed investigation of the structural properties of such grain boundaries, they can hopefully be optimised to enhance protonic conductivity in many different potential solid electrolyte materials.

Summary

Through the use of atomistic simulation techniques we have successfully shown that proton incorporation is favoured in ZrO_2 grain boundaries and that proton-trapping is significantly reduced at the grain boundary compared to the bulk structure. To the best of our knowledge, this is the first investigation of its kind with the focus on proton-doped grain boundaries in any material. By finding and analysing the lowest energy grain boundary structures we have provided a fully quantitative comparison between bulk proton-doped ZrO_2 and the Σ 5(310)/[001] and Σ 5(210)/[001] grain boundaries. Both redox reaction and hydration energies were found to be significantly reduced in the grain boundaries suggesting a far higher concentration of electronic defects at the grain boundaries. Binding energies calculated for aliovalent dopant–proton defect pairs in the grain boundaries are similar to values previously calculated for the attractive electrolyte candidate, $BaZrO_3$. The binding energy was found to be dependent on the ionic radii of the dopant ion with Sc producing the highest values and Y, Gd and La producing the smallest energies. However, La is shown to seriously distort the surrounding lattice because of its large ionic radius relative to Zr.

Acknowledgements

This research was supported by a Grant-in-Aid for Scientific Research on Innovative Areas, "Exploration of nanostructure–property relationships for materials innovation" from the Ministry of Education, Culture, Sports, Science, and Technology (MEXT) of Japan.

References

1 M. R. Ormerod, *Chem. Soc. Rev.*, 2003, **32**, 17.
2 R. D. Monte and J. Kašpar, *J. Mater. Chem.*, 2004, **15**, 633.
3 Z. J. Shen, E. Adolfsson, M. Nygren, L. Gao, H. Kawaoka and K. Niihara, *Adv. Mater.*, 2001, **13**, 214.
4 P. F. Manicone, P. R. Iommetti and L. Rafaelli, *J. Dent.*, 2007, **35**, 819.
5 H. J. Avila-Paredes, E. Barrera-Calva, H. U. Anderson, R. A. De Souza, M. Martin, Z. A. Munir and S. Kim, *J. Mater. Chem.*, 2010, **20**, 6235.
6 B. Scherrer, M. V. F. Schlupp, D. Stender, J. Martynczuk, J. G. Grolig, H. Ma, P. Kocher, T. Lippert, M. Prestat and L. J. Gauckler, *Adv. Funct. Mater.*, 2013, **23**, 1957.
7 M. Shirpour, G. Gregori, R. Merkle and J. Maier, *Phys. Chem. Phys. Chem.*, 2011, **13**, 937.
8 C. Tande, D. Perez-Coll and G. C. Mather, *J. Mater. Chem.*, 2012, **22**, 11208.
9 D. Pérez-Coll and G. C. Mather, *Solid State Ionics*, 2010, **181**, 20.
10 E. Ruiz-Trejo and J. A. Kilner, *J. Appl. Electrochem.*, 2009, **39**, 523.
11 Y. Yamazaki, F. Blanc, Y. Okuyama, L. Buannic, J. C. Lucio-Vega, C. P. Grey and S. M. Haile, *Nat. Mater.*, 2013, **12**, 647.
12 S. J. Stokes and M. S. Islam, *J. Mater. Chem.*, 2010, **20**, 6258.
13 E. Fabbri, D. Pergolesi and E. Traversa, *Chem. Soc. Rev.*, 2010, **39**, 4355.
14 J. M. Polfus, K. Toyoura, F. Oba, I. Tanaka and R. Haugsrud, *Phys. Chem. Chem. Phys.*, 2012, **14**, 12339.
15 J.-S. Lee and D.-Y. Kim, *J. Mater. Res.*, 2001, **16**, 2739.
16 X. Guo, W. Sigle, J. Fleig and J. Maier, *Solid State Ionics*, 2002, **154**, 555.
17 X. Guo and R. Waser, *Solid State Ionics*, 2004, **173**, 63.
18 X. Guo, *J. Phys. Chem. Solids*, 1999, **60**, 539.
19 S. Kim, U. Anselmi-Tamburini, H. J. Park, M. Martin and Z. A. Munir, *Adv. Mater.*, 2008, **20**, 556.
20 S. Kim, H. J. Avila-Paredes, S. Wang, C.-T. Chen, R. A. De Souza, M. Martin and Z. A. Munir, *Phys. Chem. Chem. Phys.*, 2009, **11**, 3035.
21 H. J. Avila-Paredes, C.-T. Chen, S. Wang, R. A. De Souza, M. Martin, Z. A. Munir and S. Kim, *J. Mater. Chem.*, 2010, **20**, 10110.
22 J. S. Park, Y. B. Kim, J. H. Shim, S. Kang, T. M. Gür and F. B. Prinz, *Chem. Mater.*, 2010, **22**, 5366.
23 M. J. Pietrowski, R. A. De Souza, S. Kim, Z. A. Munir and M. Martin, *Solid State Ionics*, 2012, **225**, 241.
24 T. Norby, M. Widerøe, R. Glöckner and Y. Larring, *Dalton Trans.*, 2004, 3012.
25 W. Piskorz, J. Gryboś, F. Zasada, S. Cristol, J.-F. Paul, A. Adamski and Z. Sojka, *J. Phys. Chem. C*, 2011, **115**, 24274.
26 W. Piskorz, J. Gryboś, F. Zasada, P. Zapała, S. Cristol, J.-F. Paul and Z. Sojka, *J. Phys. Chem. C*, 2012, **116**, 19307.
27 R. Añez, A. Sierraalta, G. Martorell and P. Sautet, *Surf. Sci.*, 2009, **603**, 2526.

28 S. Raz, K. Sasaki, J. Maier and I. Riess, *Solid State Ionics*, 2001, **143**, 181.
29 T. Matzke, U. Stimming, C. Karmonik, M. Soetratmo, R. Hempelmann and F. Güthoff, *Solid State Ionics*, 1996, **86**, 621.
30 M. S. Islam, P. R. Slater, J. R. Tolchard and T. Dinges, *Dalton Trans.*, 2004, 3061.
31 D. M. Duffy and P. W. Tasker, *Physica B and C*, 1985, **131**, 46.
32 D. M. Duffy, *J. Phys. C: Solid State Phys.*, 1986, **19**, 4393.
33 C. A. J. Fisher and H. Matsubara, *Comput. Mater. Sci.*, 1999, **14**, 177.
34 R. L. González-Romero, J. J. Meléndez, D. Gómez-García, F. L. Cumbrera and A. Domínguez-Rodríquez, *Solid State Ionics*, 2012, **219**, 1.
35 T. Oyama, M. Yoshiya and H. Matsubara, *Phys. Rev. B: Condens. Matter Mater. Phys.*, 2005, **71**, 224105.
36 H. B. Lee, F. B. Prinz and W. Cai, *Acta Mater.*, 2013, **61**, 3872.
37 M. Yoshiya and T. Oyama, *J. Mater. Sci.*, 2011, **46**, 4176.
38 J. Wu, R. A. Davies, M. S. Islam and S. M. Haile, *Chem. Mater.*, 2005, **17**, 846.
39 G. C. Mather and M. S. Islam, *Chem. Mater.*, 2005, **17**, 1736.
40 M. S. Islam, *J. Mater. Chem.*, 2000, **10**, 1027.
41 E. Kendrick, J. Kendrick, K. S. Knight, M. S. Islam and P. R. Slater, *Nat. Mater.*, 2007, **6**, 871.
42 J. H. Harding, *Rep. Prog. Phys.*, 1990, **53**, 1403.
43 S. M. Woodley, P. D. Battle, J. D. Gale and C. R. A. Catlow, *Phys. Chem. Chem. Phys.*, 1999, **1**, 2535.
44 K. Wang, C. Li, H. Dong, X. Ye, X. Lu and W. Ding, *Metall. Mater. Trans. A*, 2010, **41**, 3525.
45 D. Lide, *CRC Handbook of Chemistry and Physics*, CRC Press, Boca Raton, USA, 1998.
46 M. W. Chase, *NIST-JANAF Thermochemical Tables*, American Chemical Society, American Institute of Physics for the National Institute of Standards and Technology, Woodbury, USA, 1971.
47 E. V. Stefanovich, A. L. Shluger and C. R. A. Catlow, *Phys. Rev. B: Condens. Matter Mater. Phys.*, 1994, **49**, 11560.
48 G. Lewis and C. R. A. Catlow, *J. Phys. C: Solid State Phys.*, 1985, **18**, 1149.
49 L. Minervini, R. W. Grimes and K. E. Sickafus, *J. Am. Ceram. Soc.*, 2000, **83**, 1873.
50 N. F. Mott and M. J. Littleton, *J. Chem. Soc., Faraday Trans. 2*, 1989, **85**, 565.
51 J. Gale and A. Rohl, *Mol. Simul.*, 2003, **29**, 291.
52 P. Saul and C. R. A. Catlow, *Philos. Mag. B*, 1985, **51**, 107.
53 K. P. Schroder, J. Sauer, M. Leslie, C. R. A. Catlow and J. M. Thomas, *Chem. Phys. Lett.*, 1992, **188**, 320.
54 P. Panchmatia, A. Orera, J. Hanna, M. E. Smith, P. R. Slater and M. S. Islam, *J. Mater. Chem.*, 2010, **20**, 2766.
55 E. C. Dickey, X. Fan and S. J. Pennycook, *J. Am. Ceram. Soc.*, 2001, **84**, 1361.
56 K. L. Merkle, G.-R. Bai, Z. Li, C.-Y. Song and L. J. Thompson, *Phys. Status Solidi A*, 1998, **166**, 73.
57 F. Oba, I. Tanaka, S. R. Nishitani, H. Adachi, B. Slater and D. H. Gay, *Philos. Mag. A*, 2000, **80**, 1567.
58 F. Oba, H. Ohta, Y. Sato, H. Hosono, T. Yamamoto and Y. Ikuhara, *Phys. Rev. B: Condens. Matter Mater. Phys.*, 2004, **70**, 125415.
59 A. Nakamura, N. Shibata, N. Morishige, K. Matsunaga, Y. Ikuhara and T. Yamamoto, *J. Am. Ceram. Soc.*, 2005, **88**, 938.
60 N. Shibata, F. Oba, T. Yamamoto and Y. Ikuhara, *Philos. Mag. A*, 2004, **84**, 2381.
61 H. L. Tuller and N. S. Nowick, *J. Electrochem. Soc.*, 1979, **126**, 209.
62 W. C. Chueh and S. M. Haile, *Phys. Chem. Chem. Phys.*, 2009, **11**, 8144.
63 D. Eder and R. Kramer, *Phys. Chem. Chem. Phys.*, 2002, **4**, 795.
64 J. Fergus, R. Hui, X. Li, D. P. Wilkinson and J. Zhang, *Solid Oxide Fuel Cells: Materials Properties and Performance*, CRC Press, Boca Raton, USA, 2009.
65 T. H. Etsell and S. N. Flengas, *J. Electrochem. Soc.*, 1972, **119**, 1.
66 R. Glockner, M. S. Islam and T. Norby, *Solid State Ionics*, 1999, **122**, 145.
67 N. Agmon, *Chem. Phys. Lett.*, 1995, **244**, 456.
68 M. S. Islam, R. A. Davies and J. D. Gale, *Chem. Mater.*, 2001, **13**, 2049.
69 K. D. Kreuer, S. Adams, W. Munch, A. Fuchs, U. Klock and J. Maier, *Solid State Ionics*, 2001, **145**, 295.
70 P. M. Panchmatia, A. Orera, E. Kendrick, J. V. Hanna, M. E. Smith, P. R. Slater and M. S. Islam, *J. Mater. Chem.*, 2010, **20**, 2766.
71 K. Wright, R. Freer and C. R. A. Catlow, *Phys. Chem. Miner.*, 1995, **20**, 500.
72 C. R. A. Catlow, *J. Phys. Chem. Solids*, 1977, **38**, 1131.
73 T. Zacherle, A. Schriever, R. A. De Souza and M. Martin, *Phys. Rev. B: Condens. Matter Mater. Phys.*, 2013, **87**, 134104.
74 J. A. Dawson, X. Li, C. L. Freeman, J. H. Harding and D. C. Sinclair, *J. Mater. Chem. C*, 2013, **1**, 1574.
75 J. A. Dawson, C. L. Freeman, J. H. Harding and D. C. Sinclair, *J. Solid State Chem.*, 2013, **200**, 310.
76 C. L. Freeman, J. A. Dawson, J. H. Harding, L.-B. Ben and D. C. Sinclair, *Adv. Funct. Mater.*, 2013, **23**, 491.
77 R. Devanathan, S. Thevuthasan and J. D. Gale, *Phys. Chem. Chem. Phys.*, 2009, **11**, 5506.
78 L. Malavasi, C. A. J. Fisher and M. S. Islam, *Chem. Soc. Rev.*, 2010, **39**, 4370.

